

THE PROTO-PLANETARY NEBULA M1-92 AND THE SYMBIOTIC STAR MWC 560: TWO EVOLUTIONARY PHASES OF THE SAME TYPE OF OBJECT?

A. ARRIETA

Universidad Iberoamericana, Departamento de Física y Matemáticas, Prolongación Paseo de la Reforma 880, Lomas de Santa Fe,
México DF 01210, Mexico; anabel.arrieta@uia.mx

AND

S. TORRES-PEIMBERT AND L. GEORGIEV

Instituto de Astronomía, Universidad Nacional Autónoma de México, Apartado Postal 70-264, México DF 04510, Mexico

Received 2003 July 12; accepted 2004 December 17

ABSTRACT

Important similarities between the objects M1-92, a proto-planetary nebula of bipolar morphology, and MWC 560, a symbiotic star with a jet, have been found. A brief review of the previous studies for both objects is presented for the purpose of proposing mechanisms that best explain these similarities, since up to now both objects have been studied independently. From the comparison of the spectra of both objects, the existence of a jet is confirmed for the proto-planetary nebula M1-92, as well as its binary nature and the existence of a circumnuclear disk. Finally, an evolutionary sequence is proposed for the two objects where M1-92 is ~ 900 yr more evolved than MWC 560.

Subject headings: binaries: symbiotic — ISM: jets and outflows — planetary nebulae: individual (M1-92) — stars: AGB and post-AGB — stars: individual (MWC 560)

Online material: machine-readable table

1. INTRODUCTION

Symbiotic stars are considered as interacting binary stars consisting of a red giant and a hot companion that ionizes the stellar wind of the former, creating in this way physical conditions similar to those in planetary nebulae (PNs). Symbiotic stars with infrared spectra that reveal the presence of warm dust are called D type; many of these have turned out to have Mira variables as the cool component, and a few have been shown to have bipolar nebulae. It has been proposed by several authors (Lutz et al. 1989; Morris 1990; Corradi 1995; Corradi & Schwarz 1995; Schwarz & Corradi 1992; Corradi et al. 2003) that there might be an evolutionary link between symbiotic stars and at least some of the bipolar PNs. This hypothesis has emerged from studies of an increasing number of objects that have considerable overlap in the characteristics that are common. Corradi (2003) points out that, in general, the nebulae observed around symbiotic Mira variables must be composed mainly of material lost by the Mira variables, shaped by fast winds and ejecta from the hot companion and possibly from its accretion disk. Further, from the PN perspective, he presents a list of seven PNs of marked bipolar shape that show at least one of the following analogies with symbiotic stars: (1) high-density, unresolved nebular cores, (2) $H\alpha$ profiles with extended wings, and (3) rich Fe II and [Fe II] emission in generally low ionization spectra. This evidence has reinforced the idea that there is a strong link between the symbiotic Mira variables and the highly collimated bipolar PNs.

We were intrigued by the similarities of the optical spectra of M1-92, considered as a bipolar proto-planetary nebula (PPN), and MWC 560, a binary symbiotic star. Therefore, we obtained high-dispersion data to further study these objects. In this work we explore the spectroscopic similarity between M1-92 and MWC 560 and try to determine whether this similarity extends to the physical conditions in both systems. Namely, both are interacting binary systems with a hot compact source and a cold

companion, where there is evidence of anisotropic mass loss at high velocities. For this purpose in § 2 an overview of M1-92 and MWC 560 is presented; in § 3 the observations carried out are described; in § 4 the spectral characteristics of both objects are compared; in § 5 the evidence of a jet in M1-92 is advanced, it is compared to that of MWC 560, and the physical conditions present in the jets of both systems are modeled; in § 6 the binary nature of the two objects under consideration and the similarity of the geometry of the systems are discussed; in § 7 it is proposed that both objects represent the same type of system, where M1-92 is in a more advanced stage of evolution than MWC 560; and finally, in § 8 the conclusions are presented.

2. DESCRIPTION OF THE OBJECTS

2.1. *The Proto-Planetary Nebula M1-92*

Minkowski's footprint, or M1-92, originally discovered by Minkowski (1946), is a well-known PPN in which the optical, infrared, and millimetric images show two very symmetrical lobes. The optical image consists of two lobes that define an axis of symmetry and has an extension about $10''$ along its axis, with a P.A. of $\sim 131^\circ$ (approximately northwest-southeast on the plane of the sky). The angle of inclination between the axis of bipolarity and the line of sight is $\sim 57^\circ$, where the brighter northwestern lobe points toward the observer (Solf 1994). The estimated distance to this object varies between 1 and 3.5 kpc; assuming a distance of 2.5 kpc, the size of this object is 4×10^{17} cm and its luminosity is $10^4 L_\odot$ (Cohen & Kuhl 1977).

The optical spectra of the lobes and of the central star region show emission lines of H I and He I and numerous permitted neutral or once ionized metallic emission lines and forbidden lines of [O I], [N II], and [S II] that are superimposed on a stellar continuum. The broad emission lines of H I and He I and the stronger permitted metallic emissions show strong blueward absorptions (Herbig 1975; Solf 1994). The emission spectrum was explained by lines that originate near the central star and are

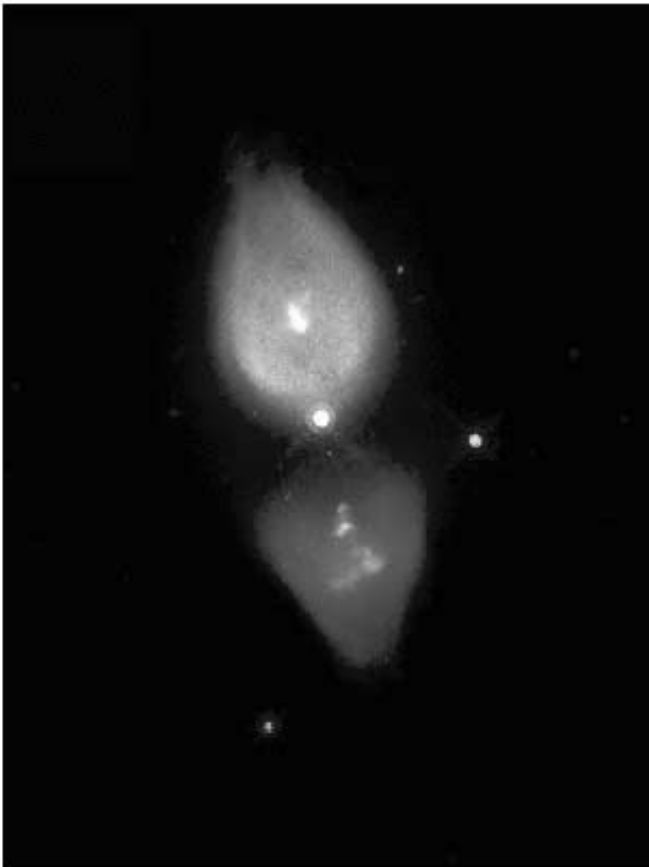


FIG. 1.—Image of M1-92 obtained with *HST* by Trammell & Goodrich (1996).

only scattered off dust being driven radially outward through the two lobes at a velocity of $\sim 31 \text{ km s}^{-1}$ (Herbig 1975). From long-slit optical spectroscopy Solf (1994) was able to separate the central emission and, by subtraction of the reflected spectrum from the dust/neutral lobes, to derive the intrinsic emission from symmetrical knots inside the lobes. Solf (1994) claimed that the intrinsic spectrum of the lobes is similar to Herbig-Haro objects, in that the latter objects show low-excitation forbidden lines ([O I], [N II], and [S II]) and faint or absent lines of high excitation ([O III], [S III]). Furthermore, Solf (1994) points out that a comparison of the observed line profiles with predictions of bow shock models from the literature indicates shock velocities in the range $200\text{--}300 \text{ km s}^{-1}$.

Spectropolarimetric studies in the knots show that the continuum and permitted emission lines are highly polarized, while the forbidden lines are not polarized (Trammell et al. 1993), in agreement with the interpretation by Herbig (1975) and Solf (1994), that the continuum and permitted emission lines are produced in the central source and are dust reflected in the lobes, and that the forbidden lines are intrinsically produced in the knots. High spatial resolution monochromatic *Hubble Space Telescope* (*HST*) images (Trammell & Goodrich 1996; Bujarrabal et al. 1998b) confirm that most of the continuum and $H\alpha$ light on the lobes is scattered from the central source and that there is intrinsic emission of faint H I, [O I], [O III], and [S II] from compact knots in both lobes along the axis of the nebula (Fig. 1). According to Bujarrabal et al. (1998b), these knots are probably associated with the propagation of shocks in a bipolar flow.

Seaquist et al. (1991), from 1667 and 1612 MHz OH maser emission maps, conclude that this emission originates in a disk

that bisects the two lobes. To explain their observations, they propose a fan-shaped disk of $2''4$ radius and of 70° opening angle located in the center of the nebula, expanding with a uniform velocity of 18 km s^{-1} . The OH would be located in a toroidal region of this disk. For a distance of 4.5 kpc they estimated a mass-loss rate in the disk of $5.6 \times 10^{-6} M_\odot \text{ yr}^{-1}$ and a kinematic age for the disk of 3000 yr (corresponding to $3.1 \times 10^{-6} M_\odot \text{ yr}^{-1}$ and 1600 yr for 2.5 kpc). This geometry is in agreement with the ring around the near-infrared peak that can be seen in the $H\text{--}K$ images by Eiroa & Hodapp (1989). This structure produces strong extinction at optical wavelengths, where Eiroa & Hodapp (1989), assuming a normal extinction law, suggest a visual extinction value of 20–22.4 mag.

In addition, the ^{13}CO high-resolution maps of Bujarrabal et al. (1998a) show a well-resolved disklike condensation in the nucleus of $2''\text{--}3''$ ($\sim 10^{17} \text{ cm}$) diameter, with an inner diameter of $\sim 1''$. This structure is essentially in expansion, with a typical velocity of $\sim 8 \text{ km s}^{-1}$. They also point out “that a disk with this inner radius and the width ($\geq 3 \times 10^{16} \text{ cm}$) derived by our fitting is unable to collimate the very narrow post-AGB jets seen in the optical.”

In addition, Bujarrabal et al. (1998a) observe in ^{13}CO a double-shell bipolar structure of molecular material external to the optical emission. The width of the shell is $\sim 0''.6$ ($2 \times 10^{16} \text{ cm}$). The velocity of the shells is larger at larger distances of the star, and the maximum deprojected velocity is $\sim 70 \text{ km s}^{-1}$. The mass of the molecular envelope is about $0.9 M_\odot$. Its kinetic moment in the axial direction and energy are $\sim 3 \times 10^{39} \text{ g cm s}^{-1}$ and $\sim 7 \times 10^{45} \text{ ergs}$, respectively. From the displacement along the axis of the emission centroid for the different velocities they estimate a total kinetic age for the nebulae of $\sim 900 \text{ yr}$. From the results derived from molecular regions, Bujarrabal et al. (1998a) propose that the shells are the remnants of the stellar envelope of the asymptotic giant branch (AGB) star accelerated by a bow-type shock wave.

The *IUE* data obtained by Feibelman & Bruhweiler (1990) revealed a hot companion. They found that the spectral distribution in the $2400\text{--}3300 \text{ \AA}$ interval is characteristic of an F2 supergiant and the residual flat UV continuum for $1200\text{--}1400 \text{ \AA}$ that can be explained by a relatively unreddened compact hot star. They concluded that the central object of M1-92 is an evolved binary system composed of a yellow supergiant and a hot compact star.

2.2. The Symbiotic Star MWC 560

The peculiar nature of MWC 560 was reported first in the Be and Ae star catalog by Merrill & Burwell (1943); they noticed a wide $\sim 1000 \text{ km s}^{-1}$ blue displaced absorption component on the H I and Ca II K lines. Sanduleak & Stephenson (1973) detected TiO bands and classified the object as an M4ep star. Its classification as a symbiotic binary is based on its emission lines, blue continuum, and red giant absorptions. Although some symbiotic systems show extended nebulosities, for MWC 560 there is only an uncertain estimate by Kohoutek (1997) of a faint small nebula through B , V , R , and $H\alpha$ filters, of $(0''.40 \pm 0''.15) \times (0''.25 \pm 0''.13)$ size, which at a distance of 1–2.5 kpc (Tomov et al. 1992; Schmid et al. 2001) corresponds to a mean diameter of $(0.5\text{--}1.2) \times 10^{16} \text{ cm}$.

Its optical spectrum shows emission lines of H I and He I and numerous permitted neutral or once ionized metallic emission lines and forbidden lines of [O I] that are superimposed on a stellar continuum that shows evidence of TiO bands. The broad emission lines of H I and He I and the stronger permitted metallic emissions show strong blueward absorptions. Bond et al.

(1984) found that the blue displaced absorption components have a complex structure that extends up to -3000 km s^{-1} ; this structure is variable on timescales of a day. High-speed optical photometry has shown rapid variations of $\pm 0.2 \text{ mag}$ in timescales of a few minutes.

From 1990 January to April, MWC 560 underwent a mass ejection episode increasing its luminosity by 2 mag. The spectra obtained by Tomov et al. (1990) during that phase showed spectacular spectral changes in the blueshifted absorption components of H I, He I, Ca II H and K, Na I D, and some permitted lines of Fe II. During the 1990 outburst, the absorption lines showed strong variability in radial velocity, sometimes reaching a value over -6000 km s^{-1} and other times as low as approximately -500 km s^{-1} . The observed line profiles can be explained by a flux of dense material at different velocities, or a jet, seen along the line of sight (Tomov et al. 1990, 1992). At present it is thought that this is a binary symbiotic system where an M giant is transferring material to a white dwarf companion. It is believed that a combination of a giant companion with high mass-loss rate ($10^{-7} M_{\odot} \text{ yr}^{-1}$) and large orbital period ($>2000 \text{ days}$) gives rise to the formation of an accretion disk with an external radius of $\sim 100 R_{\odot}$. In the inner zone of the accretion disk the gas from the jet is accelerated and collimated; to achieve this, a rotating magnetosphere has been proposed.

MWC 560 is an extraordinary object since its jet axis is practically aligned to the line of sight. Considering that jet aperture angles are about 10° , only a small fraction (1%) of the sources with a jet give the opportunity of presenting this alignment (Schmid et al. 2001). This special configuration offers a unique opportunity to complement the information about the physics involved in the acceleration and the collimation of stellar jets. Schmid et al. (2001) report that MWC 560 is the only known stellar source with this orientation.

3. OBSERVATIONS

The observations were carried out at the Observatorio Astronómico Nacional in San Pedro Mártir, Baja, California with the 2.1 m telescope and the REOSC echelle spectrograph ($R \sim 18,000$ at 5000 \AA) and a 1024×1024 Tektronix detector that yields a spectral resolution of 10.6 km s^{-1} and a spatial resolution of $0''.99 \text{ pixel}^{-1}$. The $3600\text{--}6800 \text{ \AA}$ range was covered in 29 orders. Table 1 contains the log of the observations, including exposure time and spectral resolution. The width of the slit was $150 \mu\text{m}$ placed along the east-west direction. The data reduction was carried out with IRAF routines. We normalized the spectra to the continuum for each spectral order with a Chebyshev polynomial. The normalized spectrum from 4160 to 6850 \AA is presented in Figure 2, where the most intense features have been marked.

In Table 2 we list the wavelengths and identifications of the emission features in the objects. The measured wavelengths and equivalent widths in our list refer to features in the $4160\text{--}6800 \text{ \AA}$ range because in the blue section of our data ($3600\text{--}4160 \text{ \AA}$) it is difficult to ascertain the continuum level. The line identifications were carried out following those for MWC 560 (Kolev & Tomov 1993; Chentsov et al. 1997) and for XX Oph (Merrill 1951, 1961).

3.1. M1-92

For M1-92 the slit was centered on the northwest condensation (see Fig. 1) where there is contribution of the dust-scattered light from the central region, as well as intrinsic emission from

TABLE 1
LOG OF OBSERVATIONS

Object	Observation Date	Exposure (s)	Resolution ($\text{km s}^{-1} \text{ pixel}^{-1}$)
M1-92.....	1996 Apr 23	360	10.6
	1997 Jun 10	600	10.6
	1999 Jun 10	1350	21.2
MWC 560.....	1999 Jan 19	900	10.6

the knots. This is the brightest region, and a better signal-to-noise ratio (S/N) can be achieved. In the 1999 June observations of M1-92 adjacent pixels were binned, yielding a 512×512 array to increase the S/N, and three exposures of 450 s each were combined. Both the spectrum displayed in Figure 2 and the line identifications that follow are from this combined spectrum.

In the $4160\text{--}6800 \text{ \AA}$ range the spectrum of M1-92 shows a wealth of emission lines, very intense H I, moderately intense He I, and numerous neutral or once ionized permitted metallic lines, as well as some forbidden lines. In this wavelength range we measured, or see traces of, altogether 336 emission lines, of which 28 are blends. The identifications correspond to H I (3 lines), He I (2 lines), N II (1 line), [N II] (2 lines), [O I] (3 lines), Na I (2 lines), Mg I (5 lines), Mg II (2 lines), Si II (4 lines), Sc II (19 lines), Ti I (1 line), Ti II (67 lines), V II (6 lines), Cr I (3 lines), Cr II (38 lines), Fe I (44 lines), Fe II (131 lines), Ni I (1 line), Ni II (2 lines), and Ba II (1 line); one unidentified line is also present. In our data we did not find any photospheric absorption features. Although Solf (1994) identified $\lambda 5200$ as an [N I] $\lambda 5200$ feature, in our data we were able to identify this feature as Fe II $\lambda 5197.87$ (multiplet 49). We should also point out that in the same wavelength interval Trammell et al. (1993) measure [O III] $\lambda\lambda 4959, 5007$ in the northwestern lobe, but in our data we were unable to measure it or see traces of it. No author has reported photospheric absorption lines in any of the lobes, nor in the central region.

Outstanding in the spectra are the observed profiles of the strong permitted lines H I, He I, Na I, and Fe II (multiplet 42); these profiles have complex absorption components blueshifted from their corresponding emission line. This type of profile is different from a P Cygni type since the absorption component is detached from its emission component in each line. The absorption components show maximum velocities of $580\text{--}770 \text{ km s}^{-1}$ and widths of $200\text{--}450 \text{ km s}^{-1}$.

The profiles of the strong blueward absorbed permitted lines of this object are displayed in Figure 3. Table 3 presents the identifications and terminal velocity (or maximum velocity) of the wide absorption features where the error in the velocity estimates is $\pm 10 \text{ km s}^{-1}$ (except for those with *b* and *c*, where it is not possible to estimate the error as a result of the uncertainties in the determination of the continuum).

3.2. MWC 560

Similarly, the spectrum of MWC 560 in the same wavelength interval shows very intense H I and He I emissions and numerous neutral or once ionized metallic emission lines. We measure, or see traces of, altogether 330 emission lines, of which 17 are blends, which correspond to H I (3 lines), He I (2 lines), N II (1 line), [O I] (3 lines), Mg I (5 lines), Mg II (2 lines), Si II (4 lines), Sc II (18 lines), Ti I (2 lines), Ti II (67 lines), V II (6 lines), Cr I (3 lines), Cr II (38 lines), Fe I (42 lines), Fe II (132 lines), Ni I (1 line), Ni II (1 line), and Ba II (1 line). As has been extensively reported by several authors, this is a highly variable object, and on occasion the spectrum shows very pronounced photospheric

TABLE 2
LIST OF IDENTIFIED SPECTRAL FEATURES IN THE SPECTRA OF M1-92 AND MWC 560

λ_0	M1-92		MWC 560		IDENTIFICATION
	λ_{obs}	EW	λ_{obs}	EW	
4161.52.....	4160.65	0.45	4161.84	0.33	Ti II 21
4163.64.....	4163.17	0.34	4164.08	0.39	Ti II 105
4171.90.....	4171.42	0.12	4172.33	0.34	Ti II 105
4173.45.....	4172.98	0.82	4173.92	0.63	Fe II 27
4177.70.....	4177.01	0.31	4178.06	0.36	Fe II 21
4178.86.....	4178.32	0.89	4179.29	0.76	Fe II 28
4183.20.....	4182.54	0.14	4183.81	0.08	Fe II 21
4184.33.....	4183.87	0.31	4184.75	0.12	Ti II 21
4202.03.....	4201.64	0.49	4202.59	0.35	Fe I 42*
4202.35.....					V II 25
4205.08.....	4204.82	0.68	4205.64	0.28	V II 37
4205.48.....					Fe II 22
4211.80.....	4211.09	0.16	4212.31	0.11	Fe II 21
4216.19.....	4215.51	0.45	4216.04	0.18	Fe II 3
4227.43.....	4226.29	0.45	4227.66	0.23	Fe I 693
4233.17.....	4232.54	1.52	4233.62	1.14	Fe II 27
4238.82.....	4238.33	0.26	4239.03	0.11	Fe I 693
4242.38.....	4241.85	0.26	4242.81	0.20	Cr II 31
4243.98.....	4243.18	0.30	4244.43	0.09	Fe II 21F
4244.80.....	4244.42	0.10	4245.04	0.03	Ni II 9
4246.83.....	4246.55	0.11	4247.27	0.28	Sc II 7
4252.62.....	4251.98	0.13	Tr	Tr	Cr II 31
4254.41.....	4253.78	0.06	4254.86	0.12	V II 18
4258.16.....	4257.74	0.36	4258.58	0.28	Fe II 28
4261.92.....	4261.28	0.17	4262.33	0.17	Cr II 31
4269.28.....	4368.64	0.20	4269.62	0.07	Cr II 31
4271.76.....	4271.27	0.34	4272.19	0.18	Fe I 42
4273.32.....	4272.70	0.33	4273.75	0.24	Fe II 27
4275.57.....	4274.87	0.38	4275.94	0.10	Cr II 31
4276.83.....	4276.23	0.05	4277.44	0.04	Fe II 21F
4278.13.....	4277.53	0.17	4278.57	0.09	Fe II 32
4284.21.....	4283.75	0.07	4284.67	0.08	Cr II 31
4287.40.....	4286.75	0.47	4287.99	0.50	Fe II 7F
4290.22.....	4289.7	0.39	4290.65	0.60	Ti II 41
4294.10.....	4293.67	0.12	4294.60	0.48	Ti II 20
4296.57.....	4296.00	0.36	4297.04	0.42	Fe II 28
4300.05.....	4299.55	0.34	4300.52	0.63	Ti II 41
4301.93.....	4301.35	0.20	4302.42	0.46	Ti II 41
4303.17.....	4302.64	0.58	4303.60	0.53	Fe II 27
4305.72.....	4305.29	0.12	4306.13	0.14	Sc II 15
4307.90.....	4307.33	0.28	4308.34	0.40	Ti II 41
4312.86.....	4312.30	0.32	4313.35	0.5 ^a	Ti II 41
4314.08.....	4313.60	0.40	4314.69	0.7 ^a	Sc II 15
4314.98.....	4314.38	0.27	4315.44	0.8 ^a	Ti II 41
4316.81.....	4316.09	0.31	4317.34	0.4 ^a	Ti II 94
4320.74.....	4320.23	0.28	4321.19	0.3 ^a	Sc II 15
4325.01.....	4325.19	0.51	4325.39	0.1 ^a	Sc II 15
4325.76.....			4326.24	0.1 ^a	Fe I 42
4330.26.....	4329.65	0.17	4330.89	0.3 ^a	Ti II 94
4330.71.....					Ti II 41
4337.92.....	Tr	Tr	4338.49	0.3 ^b	Ti II 20
4340.47.....	4341.17	5.52	4341.06	4.76	H I γ
4344.29.....	Tr	Tr	4344.64	0.3 ^c	Ti II 20
4351.76.....	4351.22	1.48	4352.16	0.89	Fe II 27
4354.61.....	4354.2	0.07	4354.96	0.07	Sc II 14
4359.34.....	4358.6	0.50	4359.96	0.41	Fe II 7F
4367.66.....	4367.15	0.22	4368.17	0.3	Ti II 104
4369.40.....	4368.88	0.25	4369.86	0.20	Fe II 28
4374.46.....	4374.15	0.38	4375.12	0.38	Sc II 14
4374.82.....					Ti II 93
4375.93.....	4375.34	0.21	4376.38	0.06	Fe I 2
4384.21.....	4383.88	0.5	4384.95	0.42	Fe II 36F
4385.38.....	4384.77	0.87	4385.84	0.60	Fe II 27
4386.86.....	4386.22	0.26	4387.31	0.20	Ti II 104

TABLE 2—Continued

λ_0	M1-92		MWC 560		IDENTIFICATION
	λ_{obs}	EW	λ_{obs}	EW	
4390.98.....	4390.54	0.46	4391.50	0.21	Ti II 61
4394.06.....	4394.52	0.91	4394.57	0.29	Ti II 51
4395.03.....			4395.52	0.44	Ti II 19
4395.85.....			4396.31	0.18	Ti II 61
4399.77.....	4399.31	0.57	4400.44	0.63	Ti II 51
4403.68.....	4403.79	0.97	V II 30
4404.75.....	4404.15	0.35	4405.24	0.18	Fe I 41
4409.22.....	4408.48	0.40	4409.84	0.2	Ti II 61
4411.08.....	4410.87	0.08	4411.36	0.33	Ti II 115
4413.60.....	4413.16	0.57	4414.18	0.20	Fe II 32
4413.78.....					Fe II 7F
4415.56.....	4414.55	0.33	4415.81	0.46	Sc II 14
4416.82.....	4415.92	0.76	4417.27	0.66	Fe II 27
4417.72.....	4417.37	0.57	4418.35	0.61	Ti II 40
4418.34.....					Ti II 51
4421.95.....	4421.45	0.17	4422.52	0.24	Ti II 93
4427.31.....	4426.80	0.26	4427.81	0.11	Fe II 2
4428.00.....	Tr	Tr	4428.35	0.09	Mg II 9
4441.73.....	4441.37	0.18	4442.17	0.14	Ti II 40
4442.34.....	4442.17	0.28	4442.86	0.85	Fe I 68
4443.80.....	4443.23	0.20	4444.28	0.43	Ti II 19
4444.56.....	4443.98	0.15	4444.99	0.16	Ti II 31
4450.49.....	4449.78	0.24	4450.85	0.25	Ti II 19
4452.11.....	4451.33	0.29	4452.31	0.06	Fe II 7F
4461.43.....	4460.91	0.43	4461.90	0.22	Fe II 26
4464.46.....	4463.93	0.14	4464.93	0.23	Ti II 40
4468.49.....	4468.15	0.52	4469.06	0.74	Ti II 31
4471.48.....	4470.36	0.28	4471.35	0.18	He I 14
4472.92.....	4472.32	0.35	4473.38	0.28	Fe II 37
4476.02.....	4476.86	0.11	Fe I 355
4481.13.....	4481.06	0.92	4481.73	0.29	Mg II 4
4489.18.....	4488.47	0.86	4489.64	0.45	Fe II 37
4491.40.....	4490.76	0.71	4491.92	0.53	Fe II 37
4493.53.....	4493.06	0.12	4494.00	0.08	Ti II 18
4494.57.....	4494.05	0.23	4494.96	0.10	Fe I 68
4496.86.....	4496.42	0.09	4497.46	0.10	Cr I 10
4501.27.....	4500.64	0.32	4501.76	0.46	Ti II 31
4508.28.....	4507.68	1.03	4508.76	0.79	Fe II 38
4515.34.....	4514.72	0.93	4515.80	0.70	Fe II 37
4518.30.....	4517.96	0.19	4518.79	0.10	Ti II 18
4520.22.....	4519.61	0.75	4520.66	0.5	Fe II 37
4522.63.....	4522.00	1.08	4523.07	0.75	Fe II 38
4524.93.....	4524.59	0.08	4525.15	0.28	Ba II 3
4528.51.....	4528.01	0.22	4528.99	0.10	V II 56
4529.46.....	4528.91	0.15	4529.96	0.12	Ti II 82
4533.97.....	4533.6	0.59	4534.44	0.56	Ti II 50
4539.62.....	4539.12	0.29	4540.12	0.15	Cr II 39
4541.52.....	4540.92	0.34	4541.93	0.36	Fe II 38
4545.14.....	4544.52	0.29	4545.83	0.30	Ti II 30
4549.47.....	4548.95	1.52	4550.02	1.28	Fe II 38
4552.23.....	4551.81	0.19	4552.81	0.08	Ti II 30
4555.02.....	4554.35	0.28	4555.53	0.19	Cr II 44
4555.89.....	4455.31	0.91	4556.42	0.58	Fe II 37
4558.66.....	4558.05	0.78	4559.15	0.46	Cr II 44
4563.76.....	4563.37	0.47	4564.28	0.38	Ti II 50
4571.10.....	4570.39	0.15	4571.65	0.10	Mg I 1
4571.97.....	4571.34	0.54	4572.51	0.47	Ti II 82
4576.33.....	4575.81	0.44	4576.80	0.54	Fe II 38
4579.52.....	4578.16	0.06	4579.77	0.03	Fe II
4580.06.....	4579.43	0.60	4580.58	0.21	Fe II 26
4582.84.....	4583.09	2.23	4583.46	0.52	Fe II 37
4583.83.....			4584.40	1.13	Fe II 38*
4588.22.....	4587.63	0.29	4588.74	0.54	Cr II 44
4589.89.....	4589.32	0.22	4590.48	0.26	Cr II 44
4592.09.....	4591.61	0.31	4592.61	0.17	Cr II 44

TABLE 2—Continued

λ_0	M1-92		MWC 560		IDENTIFICATION
	λ_{obs}	EW	λ_{obs}	EW	
4596.06.....	4595.32	0.33	4596.48	0.08	Fe I 820?
4600.19.....	4597.87	0.12	Tr	Tr	V II 56
4601.34.....	4601.06	0.18	Tr	Tr	Fe II 43
4602.94.....	4602.31	0.30	Tr	Tr	Fe I 39
4616.64.....	4616.09	0.34	4617.08	0.18	Cr II 44
4618.83.....	4618.22	0.52	4619.27	0.35	Cr II 44
4620.51.....	4619.85	0.58	4620.97	0.25	Fe II 38
4629.34.....	4628.77	1.67	4629.78	0.90	Fe II 37
4634.11.....	4633.54	0.56	4634.54	0.32	Cr II 44
4635.33.....	4634.92	0.31	4635.76	0.11	Fe II 186
4636.34.....	4635.84	0.19	4636.72	0.05	Ti II 38
4648.93.....	4648.30	0.28	4649.43	0.04	Fe II 25
4656.97.....	4656.36	0.67	4657.63	0.33	Fe II 43
4663.70.....	4662.94	0.38	4664.23	0.07	Fe II 44
4666.75.....	4666.18	0.74	4667.30	0.29	Fe II 37
4670.17.....	4669.58	0.40	4670.80	0.28	Fe II 25
4698.47.....	4698.02	0.30	4699.08	0.11	Cr I 186?
4702.98.....	4702.49	0.14	4703.60	0.17	Mg I 11
4708.66.....	4708.33	0.15	4709.14	0.14	Ti II 49
4728.07.....	4727.59	0.45	4728.72	0.14	Fe II 4F
4731.44.....	4730.79	0.84	4731.93	0.42	Fe II 43
4762.77.....	4761.99	0.19	4763.30	0.09	Ti II 17
4763.84.....	4763.79	0.45	4764.46	0.17	Ti II 48
4764.54.....	4765.14	0.11	Ti II 48
4779.99.....	4779.46	0.25	4780.57	0.28	Ti II 92
4781.72.....	4782.17	0.46	Ti I 41?
4798.54.....	4797.85	0.39	4799.08	0.16	Ti II 17
4805.10.....	4804.68	0.35	4805.62	0.32	Ti II 92
4812.35.....	4811.83	0.25	4812.79	0.07	Cr II 30
4814.55.....	4813.78	0.35	4815.03	0.09	Fe II 20F
4824.14.....	4823.46	0.51	4824.61	0.43	Cr II 30
4825.71.....	4825.12	0.19	4826.08	0.04	Fe II 30
4830.84.....	4830.55	0.13	4831.2	0.2 ^a	Cr I
4833.21.....	4432.62	0.53	4833.74	0.2 ^a	Fe II 30
4836.22.....	4835.73	0.14	4836.81	0.8 ^a	Cr II 30
4848.24.....	4847.91	0.62	Tr	Tr ^a	Cr II 30
4861.33.....	4861.16	18.6	4862.23	15.8	H I β
4871.27.....	4870.6	0.26	4871.83	0.1 ^c	Fe II 25
4874.02.....	4873.53	0.14	4874.63	0.17	Ti II 114
4876.41.....	4875.81	0.32	4877.03	0.19	Cr II 30
4884.57.....	4883.94	0.18	4884.46	0.25	Cr II 30
4889.63.....	4888.94	0.36	4890.19	0.08	Fe II 4F
4889.70.....	4890.52	0.24	Tr	Tr	Fe II 3F
4893.78.....	4893.21	0.38	4894.47	0.07	Fe II 36
4905.35.....	4904.58	0.06	4906.00	0.28	Fe II 20F
4911.20.....	4910.56	0.18	4911.76	0.28	Ti II 114
4923.92.....	4923.39	3.94	4924.47	2.09	Fe II 42
.....	4938.86	0.36
4954.....	Tr	Tr	TiO band
4957.30.....	4956.86	0.33	4958.13	0.09	Fe I 318
4957.60.....	Fe I 318
4991.11.....	4990.48	0.21	4991.7	0.04 ^a	Fe II 25
4993.36.....	4992.89	0.62	4993.96	0.20 ^a	Fe II 36
5001.87.....	5000.79	0.49	5002.02	0.12	Fe I 965
5005.17.....	5004.87	0.31	5005.82	0.11	Ti II 71
5013.71.....	5013.07	0.17	5014.16	0.30	Ti II 71
5018.43.....	5017.91	3.34	5019.06	2.83	Fe II 42
5031.02.....	5030.46	0.20	5031.58	0.20	Sc II 23
5041.06.....	5040.82	0.42	5041.88	0.09	Si II 5
5068.86.....	5068.45	0.27	Sc II
5072.40.....	5071.95	0.25	5072.92	0.15	Fe II 19F
5077.23.....	5078.95	0.43	Fe I 66?
5083.34.....	5082.78	0.19	Fe I 16?
5100.66.....	5100.07	0.53	5101.35	0.17	Fe II 35
5100.70.....	Fe II

TABLE 2—Continued

λ_0	M1-92		MWC 560		IDENTIFICATION
	λ_{obs}	EW	λ_{obs}	EW	
5100.84.....					Fe II 185
5107.45.....	5106.93	0.34	5108.23	0.06	Fe I 16
5110.64.....	5109.81	0.26	5110.95	0.04	Fe I 1
5129.14.....	5128.58	0.31	5129.80	0.33	Ti II 86
5132.67.....	5132.96	0.56	5133.30	0.18	Fe II 35
5136.76.....	5163.27	0.31	5137.40	0.04	Fe II 35
5146.12.....	5145.39	0.28	5146.69	0.05 ^a	Fe II 35
5154.06.....	5153.59	0.48	5154.69	0.36	Ti II 70
5154.40.....					Fe II 35
5158.81.....	5157.96	0.27	5159.36	0.18	Fe II 19F
5167.32.....	Tr	Tr	5168.13	0.5	Mg I 2
5167.49.....	Tr	Tr			Fe I 37
5169.03.....	5168.55	2.62	5169.70	2.11	Fe II 42
5171.62.....	5171.05	0.58	5172.22	0.19	Fe II 35
5172.68.....	5172.25	0.52	5173.34	0.42	Mg I 2
5183.60.....	5183.03	0.85	5184.21	0.60	Mg I 2
5185.90.....	5185.14	0.23	5186.56	0.24	Ti II 86
5188.70.....	5188.17	0.24	5189.34	0.45	Ti II 70
5197.57.....	5197.08	1.75	5198.22	1.09	Fe II 49
5227.19.....	5226.32	0.51	5227.30	0.55	Fe I 37
5234.62.....	5234.03	1.52	5235.30	1.17	Fe II 49
5237.34.....	5236.65	0.27	5238.00	0.28	Cr II 43
5254.92.....	5254.35	0.45	5255.57	0.26	Fe II 49
5256.89.....	5256.2	0.22	5257.54	0.1	Fe II 41
5261.61.....	5261.09	0.45	5262.45	0.28	Fe II 19F
5262.10.....					Ti II 70
5264.80.....	5264.04	0.47	5265.44	0.32	Fe II 48
5268.88.....	5268.94	0.51	5269.25	0.12	Fe II 18F
5269.54.....			5270.19	0.16	Fe I 15
5272.41.....	5272.63	0.44	5273.03	0.07	Fe II 185
5273.38.....			5274.02	0.13	Fe II 18F
5274.99.....	5275.33	1.58	5275.76	0.34	Cr II 43
5275.99.....			5276.68	0.78	Fe II 49
5279.92.....	5279.33	0.35	5280.65	0.14	Cr II 43
5280.08.....					Cr II 43
5284.09.....	5283.53	1.14	5284.76	0.71	Fe II 41
5305.85.....	5305.31	0.19	5306.51	0.11	Cr II 24
5308.44.....	5307.44	0.26	5309.09	0.07	Cr II 43
5313.59.....	5313.2	0.15	5314.24	0.14	Cr II 43
5316.61.....	5316.09	2.82	5317.33	1.72	Fe II 49
5316.78.....					Fe II 48
5325.56.....	5324.87	0.53	5326.23	0.25	Fe II 49
5328.04.....	5327.63	0.52	5328.79	0.14	Fe I 15
5328.53.....					Fe I 37
5333.65.....	5332.66	0.43	5334.34	0.09	Fe II 19F
5334.88.....	5334.11	0.20	5335.54	0.13	Cr II 43
5336.81.....	5336.68	0.72	5337.47	0.32	Ti II 69
5337.71.....			5338.42	0.12	Fe II 48
5346.56.....	5345.74	0.23	5347.09	0.12	Fe II 49
5362.86.....	5362.27	1.31	5363.54	0.90	Fe II 48
5369.30.....	5369.12	0.43	5370.28	0.06	Cr II 29
5371.49.....	5371.10	0.25	5372.23	0.10	Fe 15
5376.47.....	5375.86	0.19	5377.1	0.04	Fe II 19F
5381.02.....	5380.27	0.32	5381.66	0.24	Ti II 69
5396.30.....	5396.08	0.67	5396.89	0.08	Ti II 80
5396.59.....					Ti II 102
5407.62.....	5407.1	0.31	5408.29	0.06	Cr II 23
5414.09.....	5413.57	0.59	5414.78	0.15	Fe II 48
5418.80.....	5418.41	0.12	5419.48	0.17	Ti II 69

TABLE 2—Continued

λ_0	M1-92		MWC 560		IDENTIFICATION
	λ_{obs}	EW	λ_{obs}	EW	
5420.90.....	5420.45	0.34	5421.63	0.09	Cr II 23
5425.27.....	5424.62	0.77	5425.95	0.34	Fe II 49
5427.83.....	5427.37	0.10	5428.49	0.08	Fe II
5429.70.....	5429.14	0.27	5430.39	0.09	Fe I 15
5432.98.....	5432.27	0.12	5433.7	0.17	Fe II 55
5446.92.....	5446.21	0.22	Fe I 15
5448.....	Tr	Tr	TiO band
5455.61.....	5455.11	0.25	5456.3	0.10	Fe I 15
5477.45.....	5476.23	0.39	5477.68	0.12	Cr II 50
5478.35.....	5477.73	0.24	5479.05	0.09	Cr II 50
5497.52.....	5496.84	0.18	5498.13	0.09	Fe I 15
5502.05.....	5501.15	0.26	5502.74	0.10	Cr II 50
5503.18.....	5502.50	0.15	5503.99	0.05	Cr II 50
5506.78.....	5506.16	0.16	5507.48	0.02	Fe I 15
5508.60.....	5508.11	0.11	5509.38	0.07	Cr II 50
5510.68.....	5510.1	0.20	5510.9	0.18	Cr II 23
5525.14.....	5524.62	0.18	5525.86	0.06	Fe II 56
5526.81.....	5526.50	0.49	5527.63	0.31	Sc II 31
5529.94.....	5529.25	0.31	5530.63	0.04	Ti II 68
5529.94.....					Fe II 224*
5534.86.....	5534.22	1.32	5535.56	0.63	Fe II 55
5567.82.....	5567.15	0.18	5568.49	0.06	Fe II
5569.62.....	5569.12	0.19	5570.42	0.01	Fe I 686
5572.85.....	5572.22	0.15	5573.58	0.05	Fe I 686
5577.35.....	5577.29	1.68	5577.39	0.46	O I 3F
5586.76.....	5586.59	0.54	5587.61	0.10	Fe I 686
5591.38.....	5591.35	0.28	Tr	Tr	Fe II 55
5615.65.....	5614.98	0.30	5616.29	0.09	Fe I 686
5627.49.....	5626.89	0.23	5628.26	0.07	Fe II 57
5640.97.....	5640.48	0.90	5641.72	0.12	Sc II 29
5657.87.....	5657.53	0.56	5658.73	0.36	Sc II 29*
5657.92.....					Fe II 57
5662.95.....	5662.14	0.10	5663.65	0.18	Y II 38
5667.16.....	5666.39	0.18	5667.89	0.10	Sc II 29
5669.03.....	5668.26	0.34	5669.73	0.12	Sc II 29
5684.19.....	5683.57	0.32	5684.94	0.15	Sc II 29
5709.38.....	5708.95	0.31	5710.09	0.11	Fe I 686
5712.15.....	5711.44	0.19	Tr	Tr	Fe I 686
5747.88.....	5747.10	0.20	Tr	Tr	Fe II 164
5813.67.....	5812.48	0.31	Tr	Tr	Fe II 163
5875.63.....	5875.04	0.26 ^a	Tr ^a	Tr ^a	He I 11
5889.95.....	5890.22	0.28	Na I 1
5895.92.....	5896.27	0.30	Na I 1
5952.55.....	5951.83	0.15	5953.42	0.11	Fe II 182
5957.61.....	5956.09	0.21	Tr	Tr	Si II 4
5991.38.....	5990.71	1.09	5992.21	0.48	Fe II 46
6084.11.....	6083.44	0.72	6084.90	0.22	Fe II 46
6113.33.....	6112.57	0.28	6114.15	0.09	Fe II 46
6129.71.....	6128.8	0.38	6130.40	0.11	Fe II 48
6147.74.....	6146.85	0.58	6148.61	0.42	Fe II 74
6149.24.....	6148.54	0.85	6150.14	0.28	Fe II 74
6191.59.....	6190.83	0.59	6192.33	0.09	Fe I 169
6229.34.....	6228.62	0.16	6230.07	0.04	Fe II 34
6230.73.....	6230.03	0.24	6231.58	0.06	Fe I 207
6238.38.....	6238.35	1.10	6239.26	0.49	Fe II 74
6239.95.....			6240.62	0.15	Fe II 34
6245.63.....	6244.94	0.06	6246.45	0.11	Sc II 28
6247.56.....	6246.89	0.97	6248.41	0.75	Fe II 74
6252.56.....	6251.93	0.15	6253.45	0.04	Fe I 169

TABLE 2—Continued

λ_0	M1-92		MWC 560		IDENTIFICATION
	λ_{obs}	EW	λ_{obs}	EW	
6264.82.....	6264.50	0.13	6265.35	0.08	Ti I 144
6270.24.....	6269.24	0.32	6270.79	0.05	Fe I 342
6279.76.....	6279.59	0.30	6280.62	0.07	Sc II 28
6300.30.....	6299.6	3.39	6301.11	0.73	O I 1F
6314.29.....	6313.96	0.27	Ni II 67?
6317.98.....	6316.96	0.92	6318.83	0.21	Fe II
6320.85.....	6319.77	0.16	6321.45	0.05	Sc II 28
6327.60.....	6326.62	0.33	6328.30	0.08	Ni I 44?
6331.97.....	6331.04	0.42	6332.79	0.07	Fe II 199
6335.33.....	6335.06	0.50	Tr	Tr	Fe I 62?
6347.09.....	6346.42	0.74	6348.02	0.15	Si II 2
6363.85.....	6363.17	1.03	6364.61	0.17	O I 1F
6369.45.....	6368.84	0.70	6370.28	0.22	Fe II 40
6371.36.....	6370.51	0.24	6372.18	0.08	Si II 2
6383.75.....	6383.98	0.88	6384.56	0.09	Fe II 41
6385.47.....	6386.28	0.04	Fe II
6393.60.....	6392.92	0.24	Tr	Tr	Fe I 168
6400.33.....	6399.4	0.42	Tr	Tr	Fe I 13?
6411.65.....	6410.92	0.12	Tr	Tr	Fe I 816
6407.30.....	6406.63	0.33	6408.04	0.06	Fe II 74
6416.90.....	6416.23	0.80	6417.82	0.39	Fe II 74
6430.85.....	6430.23	0.29	6431.87	0.02	Fe I 62
6432.65.....	6432.01	1.6	6433.57	0.58	Fe II 40
6442.97.....	6442.71	0.15	Tr	Tr	Fe II
6456.38.....	6455.62	1.52	6457.23	0.92	Fe II 74
6462.73.....	6461.69	0.17	6462.98	0.12	Fe I 13
6482.07.....	6481.33	0.27	6483.11	0.05	N II 8
6491.28.....	6490.31	0.32	6492.43	0.18	Ti 91
6493.05.....	6493.88	0.23	6494.00	0.06	Fe II
6506.33.....	6507.42	0.06	Fe II
6516.05.....	6515.23	2.06	6516.99	0.67	Fe II 40
6548.05.....	6545.56	0.73	N II 1F
6562.92.....	6562.46	74	6564.38	92	H α
6583.45.....	6581.22	2.85	N II 1F
6610.58.....	6611.94	0.30	N II 31?
6681.....	Tr	Tr	TiO band
6716.44.....	6714.27	0.56	S II 2F blue component
6716.44.....	6716.65	0.71	S II 2F red component
6730.82.....	6728.69	1.12	S II 2F blue component
6730.82.....	6731.08	0.67	S II 2F red component
6782.....	Tr	Tr	TiO band

NOTE.—Values derived from a combination of two lines are listed in the row for the first of the pair. Table 2 is also available in machine-readable form in the electronic edition of the *Astrophysical Journal*.

^a Affected by a near absorption line.

^b Affected by a strong near emission line.

^c Affected by wings in a near hydrogen line.

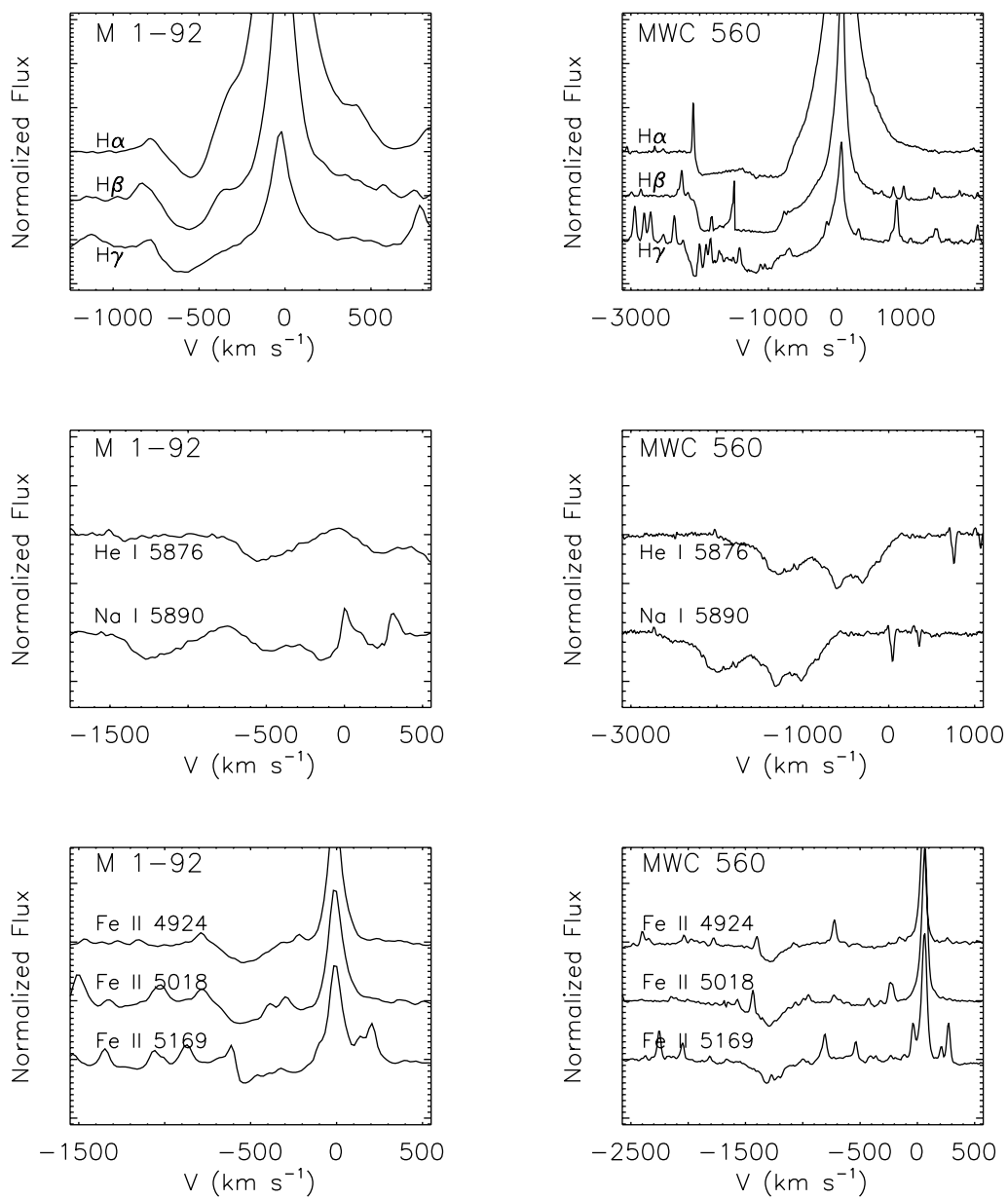


FIG. 3.—Selection of wide absorption features observed in the spectra. On the left side, the M1-92 lines are shown with a velocity of $\sim 700 \text{ km s}^{-1}$. The right column corresponds to the observed lines in MWC 560, which show a maximum velocity of $\sim 1900 \text{ km s}^{-1}$.

TABLE 3
CHARACTERISTICS OF THE WIDE ABSORPTION LINE PROFILES AND ESTIMATED JET COLUMN DENSITIES FOR THE DIFFERENT IONS

λ (Å)	IDENTIFICATION	f_{jk}^a	M1-92 (1999 June)			MWC 560		
			V_{\max} (km s ⁻¹)	EW (Å)	N_j (cm ⁻²)	V_{\max} (km s ⁻¹)	EW (Å)	N_j (cm ⁻²)
3770.....	H11	0.0028	700 ^b	b	b	1580	b	b
3797.....	H10	0.0038	730	b	b	1950	b	b
3835.....	H9	0.0052	680 ^b	b	b	>1680 ^b	b	b
3889.....	H8	0.0080	740	b	b	2000	b	b
3937.....	Ca II K	0.663	740 ^b	b	b	1900	b	b
3970.....	He	0.013	740 ^c	2.55	1.4×10^{15}	1900	10.9	$>6.2 \times 10^{15}$
4102.....	H δ	0.022	770	2.57	7.8×10^{14}	2080	10.7	$>3.2 \times 10^{15}$
4340.....	H γ	0.044	700	2.88	3.9×10^{14}	2130	13.9	$>1.9 \times 10^{15}$
4861.....	H β	0.119	750	3.57	1.4×10^{14}	2090	15.7	$>6.3 \times 10^{14}$
4924.....	Fe II	0.010	730	1.44	6.8×10^{14}	1800	1.1	5.2×10^{14}
5018.....	Fe II	0.015	740	1.83	5.6×10^{14}	1900	1.2	3.7×10^{14}
5169.....	Fe II	0.019	580	2.22	5.0×10^{14}	1640	2.2	$>5.0 \times 10^{14}$
5876.....	He I	0.610	760	1.88	1.0×10^{13}	1880	^d	^d
5890.....	Na I	0.647	670 ^c	^d	^d	>1600 ^c	^d	^d
5896.....	Na I	0.325	>650 ^c	^d	^d	>1520 ^c	^d	^d
6563.....	H α	0.640	720	4.80	2.0×10^{13}	2140	16.0	$>6.6 \times 10^{13}$

^a Oscillator strengths are from compilation by Wiese et al. (1966, 1969) and Fuhr et al. (1981).

^b Problems identifying the continuum.

^c Problems identifying maximum velocity.

^d Heavy blending.

H I and Ti II absorptions, while in other circumstances there are not significant absorptions. In our data the spectrum does not have strong photospheric absorptions and is similar to that of 1990 January presented by Kolev & Tomov (1993), where the photospheric features are less conspicuous; the only photospheric absorption features that we identify are TiO bands ($\lambda\lambda$ 4954, 5448, 6681, and 6782).

In addition, the observed profiles of the strong permitted lines are noticeable in that they have complex absorption components blueshifted from their corresponding emission line. The absorption components show maximum velocities of 1580–2140 km s⁻¹ and widths of 500–1400 km s⁻¹.

4. SPECTRAL COMPARISON OF M1-92 AND MWC 560

Despite the different nature of the two objects, a PPN and a symbiotic star, there are striking similarities between their optical spectra. They show the same permitted emission-line spectra (there is coincidence in 329 of the 342 emission lines measured); moreover, both objects show blueward detached absorption troughs in the strong permitted lines H I, He I, Na I, and Fe II (multiplet 42).

It should be noted that in our data not only is there coincidence in the emission lines present in both objects, but although in general the emission lines in M1-92 are relatively stronger than those in MWC 560, there is substantial agreement between the Fe I, Fe II, Cr II, and Sc II line intensities normalized to the continuum common to both objects. However, in the case of the Si II line intensities, there is considerable scatter in the relative ratios; we attribute most of the disagreement to the underlying photospheric Si II lines in absorption reported by Kolev & Tomov (1993) but undetected in our data.

A comparison of the profiles of the strong blueward absorbed permitted lines for the two objects is displayed in Figure 3, and the identifications and terminal velocity are given in Table 3. As pointed out, the absorption component profiles are similar in nature but not identical to each other; for M1-92 the maximum velocity and width of the absorption component are 580–770 km

s⁻¹ and 200–450 km s⁻¹ wide, respectively, while for MWC 560 they are 1580–2140 km s⁻¹ and 500–1400 km s⁻¹ wide. The presence of the permitted low-ionization emission lines indicates relatively high density gas very close to the exciting star, and the blueward detached absorption can be interpreted as evidence of a jet, as is discussed in the next section.

Although there are many similarities, there are several spectral differences that should be pointed out: (1) there are photospheric features present in the spectrum of MWC 560, TiO molecular bands and Ti II (the latter reported by Kolev & Tomov 1993), while there are none in M1-92; (2) there are moderately strong nebular emission lines [S II] $\lambda\lambda$ 6717, 6731 and [N II] $\lambda\lambda$ 6548, 6583 present in M1-92 that are very weak or absent in MWC 560; and (3) the blueward displaced absorption features in MWC 560 are at higher velocities and, moreover, have been known to be highly variable (e.g., Tomov et al. 1992), while there is no evidence of variability in M1-92. These differences are easily understandable. The cool stellar component in M1-92 is an F2 Ia-type star that does not show TiO bands, in contrast to the cool component of MWC 560, which is an M giant (see § 6). In addition, M1-92 has a well-developed molecular nebula (Bujarrabal et al. 1998a) where there are shocks that give rise to the low-ionization forbidden lines, while MWC 560 only shows traces of extended emission (Kohoutek 1997). The differences in the blueward displaced absorption features are discussed in the following section.

Raman scattering effects as evidenced in the very extended wings of H α and H β have been shown to be present in several symbiotic stars (e.g., Lee 2000) and in young PNs (e.g., Lee & Hyung 2000; Arrieta & Torres-Peimbert 2003). In several cases they are accompanied by faint $\lambda\lambda$ 6545 and 6825 features. In MWC 560 the presence of wide H α and H β emission lines, attributed to Raman-scattered Ly β and Ly γ , has been pointed out by Schmid et al. (2001). Similarly, in M1-92 the very extended wings of H α have already been identified as Raman scattering (Arrieta & Torres-Peimbert 2003). Although our spectra of both objects show marginal traces of λ 6545 corresponding to Raman-scattered

Ly γ , it is difficult to ascertain its presence; in MWC 560 it would be on the H α absorption trough, and in M1-92 it blends with [N II].

5. JETS IN M1-92 AND MWC 560

5.1. Spectroscopic Evidence

A typical P Cygni-type profile is produced in a spherically symmetric outflow where a star ejects equal amounts of material moving toward the observer and in the opposite direction. In such cases, the absorption component has its blue wing formed at the maximum negative velocity of the outflow and the emission component has its red wing extended up to the same maximum, although positive, velocity. The transition between the absorption and emission is smooth, since they are generated in the same outflow. As it has been noted, neither M1-92 nor MWC 560 exhibits typical P Cygni profiles, and in both objects the strong permitted emission line profiles of H I, He I, Na I, Ca II, and Fe II show an emission component and a much wider detached blue wing absorption component that extends several hundred to one thousand kilometers per second (see Fig. 3).

A possible explanation for this anomaly is that the system is observed pole-on. In this case the detached absorption components are formed in a jet and represent its velocity field, while the emission components are formed in the circumstellar region. Tomov et al. (1990, 1992) proposed this mechanism to explain the nature of the MWC 560 absorption features. Since both objects show similar profiles, it has been argued that for MWC 560 this detached absorption trough is the signature of a jet along the line of sight. In this work it is proposed that these features in M1-92 are also produced by a jet. If this is the case, the orientation required is in contradiction with the inclination to the line of sight derived ($\sim 57^\circ$). However, it is possible to reconcile this apparent contradiction by assuming that the spectral absorption features originate in the central region and its light reaches us after being scattered by the knots. The scattering effect on the light gives us the same observing conditions along the jet axis as in the case of MWC 560. Figure 4 shows schematically the location of the observer relative to a similar geometry in both systems.

This interpretation in M1-92 is compatible with spectropolarimetric measurements by Trammell et al. (1993) where they decomposed the spectrum for the northwestern lobe in a scattered component (originating in the central region and scattered by dust in our direction) that shows the blue absorption profiles of the Balmer and Fe II lines and an unscattered nebular component emitted by the lobe itself.

5.2. Jet Column Densities

As a first step we follow the treatment by Schmid et al. (2001), who derived the column densities in the jet from their day 144 observations of MWC 560. In a similar manner, we can derive lower limits to the jet column densities for both objects. Column densities are obtained by assuming that the absorbing gas is optically thin, only absorbs the continuum emission, and is smoothly distributed in front of the continuum source. In this case column densities for the ions in the different levels are proportional to the measured EW (in Å) according to

$$N_j = (1.13 \times 10^{20} / \lambda^2 f_{ij}) EW. \quad (1)$$

The jet column densities of the different ions derived from the wide absorption line profiles are listed in Table 3, where the identification, oscillator strength, equivalent width of absorption, and jet column densities, N_j , are included.

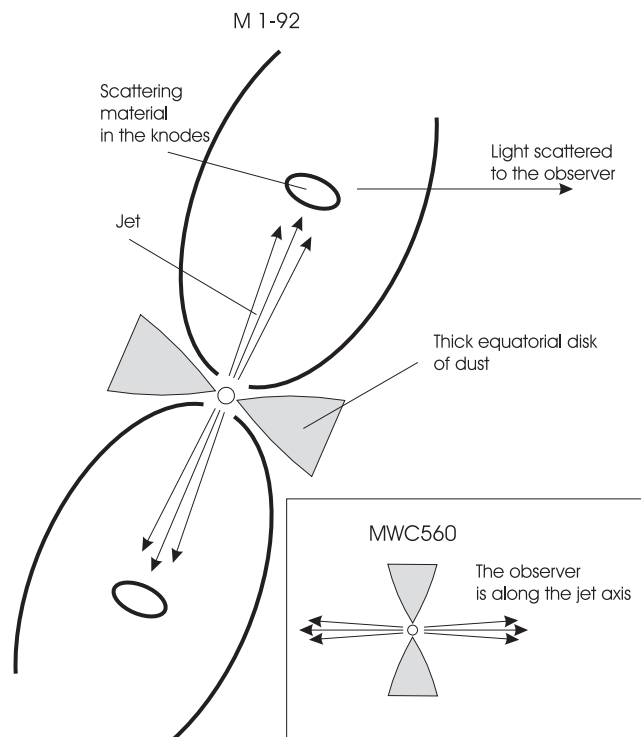


FIG. 4.—Artistic conception of the structure of M1-92 and MWC 560. In the case of M1-92 the axis jet is inclined $\sim 57^\circ$ relative to the observer, but by dust scattering we can see the light from the central object as if we were located “pole-on.” In the case of MWC 560 the jet is along the line of sight.

These values are lower limits to the column densities because the absorption lines are heavily saturated and we neglected the emission that can fill part of the absorption component. Even if these values are only approximate, the column densities of M1-92 appear to be lower than those of MWC 560; this difference is consistent with a difference in mass-loss rate of the giant companion, since the mass-loss rate in the AGB phase is larger (presumably the phase of MWC 560) than in the post-AGB phase (which is the case for M1-92).

5.3. Modeling of the Lines Formed in the Jet

One of the main ideas in this paper is that the jets in both MWC 560 and M1-92 are observed along the line of sight, resulting in peculiar profiles in the hydrogen lines and in other strong lines. Following this idea, we attempt to model the conditions for the formation of the H β line profiles in the spectra of both objects by assuming that they are produced in a jet along the line of sight. In the code used for modeling the profile the opacity in a given line is assumed to be proportional to the density, the source function is calculated from Sobolev’s approximation, and the emitted flux is obtained from the formal solution of the transport equation in three dimensions. This code has been described by Georgiev & Koenigsberger (2004).

The spectra of both objects are dominated by the Balmer lines. Under this regime it is possible to assume that the physical conditions in the jet favor the population of the second level of hydrogen. Then, the opacity $\chi_{H\beta}$ of H β as a function of distance to the central star z could be assumed to be simply proportional to the density $\rho(z)$ at the same distance. The density and velocity in a moving medium are related by the continuity law. Then, the shape of the line profile is governed by the distribution of the velocity along the jet and the mass-loss rate. We calculate the velocity $V(z)$ following Hollis & Koupelis (2000), who assume

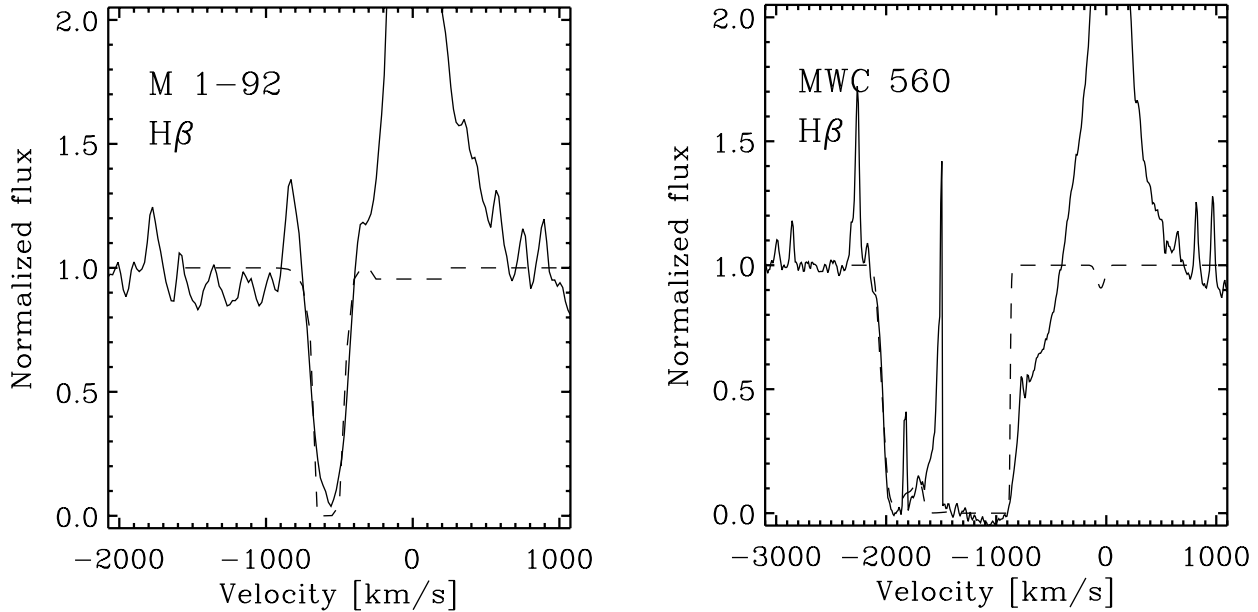


FIG. 5.—Fit to the observed H β profiles. *Solid line*: observed profile; *dashed line*: best-fit model.

that the jet is formed by discrete gas parcels rotating with angular velocity Ω_0 with density ρ_0 that are injected into the jet with velocity V_0 at some point at a distance Z_0 from the star's center. The gas is then accelerated by a magnetic field with strength B_0 . If z is the coordinate along the jet axis and $x = z/Z_0$, $v(x) = V(z)/V_0$, and $\omega(x) = \Omega(z)/\Omega_0$ are dimensionless parameters describing the position, velocity, and angular velocity of a parcel in the jet, respectively, then its equation of motion can be written (eqs. [16] and [17] of Hollis & Koupelis 2000)

$$\frac{dv}{dx} = C \frac{(1 - \omega)^2}{v^3}, \quad (2)$$

$$\frac{d\omega}{dx} = -2 \frac{\omega}{x} + D \frac{1 - \omega}{v^2 x^2}. \quad (3)$$

In these relations, the constants C and D are defined as

$$C = \frac{3Z_0^2 (B_0 \Omega_0)^2 \tan \psi}{32\pi \rho_0 V_0^4}, \quad (4)$$

$$D = \frac{3B_0^2}{8\pi \rho_0 V_0^2 \tan \psi}, \quad (5)$$

where ψ is the opening angle of the jet.

As a first step we assume a standard mass of the white dwarf $M_{\text{star}} = 0.6M_\odot$ for both objects. We also assume a constant dispersion of the velocity V_{turb} along the jet. This is a parameter that describes the width of the Doppler profile of the line in the comoving frame. It is similar to the thermal velocity in a static medium, but, because of the presence of shock inside the jet, it might be greater than the speed of sound. In addition, we fix the opening angle to be $\psi = 10^\circ$.

Then we adjust the injection velocity V_0 until we reproduce the red wing of the absorption component. We assume that V_0 is the escape velocity at the injection point so, together with M_{star} , it defines the distance Z_0 . Our model assumes an instantaneous increase of the velocity at the injection point. The red wing of the observed profile suggests some gradual increase of the velocity and density. There is no simple way for modeling that velocity

profile, so we prefer not to reproduce the exact shape of the wing but rather to keep the number of free parameters low. We note that the observed velocity is smaller than V_0 owing to the presence of chaotic motions described by the velocity dispersion V_{turb} . The wing of the profile is extended up to $V_0 - 3V_{\text{turb}}$ corresponding to the wing of a Gaussian profile, center at V_0 .

Having fixed the injection velocity, we are left with three more parameters: the density at the injection point, ρ_0 , the angular velocity, Ω_0 , and the strength of the magnetic field, B_0 . The density inside the jet is proportional to x^{-3} (Hollis & Koupelis 2000). The mass-loss rate, \dot{M} , is determined by the density at the injection point, together with V_0 . For MWC 560 the observed absorption component of H β is saturated, so only a lower limit to the mass-loss rate can be set. Following Hollis & Koupelis (2000), we relate Ω_0 to the orbital motion of the systems. Iijima (2002) determined a period of 1930 days in the brightness of MWC 560 associated with the periastron passage and the orbital period of the system. Therefore, a lower limit for Ω_0 can be obtained assuming 100% synchronization between the rotation and the orbital motion of the white dwarf that corresponds to $\Omega_0 = 2\pi/P_{\text{orb}} = 3.8 \times 10^{-8} \text{ rad s}^{-1}$. An upper limit for Ω_0 is more difficult to establish; we set a limit at $3.8 \times 10^{-6} \text{ rad s}^{-1}$, which corresponds to 1% synchronization. There is no estimate of the orbital motion of the central system of M1-92. As is seen from equations (4) and (5), the strength of the magnetic field B_0 and the rotational velocity Ω_0 enter as products. It is not possible to determine them separately for M1-92; thus, we assume for this object the same value as that of MWC 560, $\Omega_0 = 3.8 \times 10^{-8}$. One has to bear in mind that if Ω_0 increases, the magnetic field decreases, and vice versa. Finally, assuming that the gas in the jet is accelerated by the magnetic field, we can estimate the strength B_0 needed to accelerate the gas to the observed velocity of the blue wing of the absorption profile.

The entire procedure of the fit is as follows. We fix the mass of the star and the rotational velocity Ω_0 . Then we adjust “by eye” V_0 , ρ_0 , B_0 , and V_{turb} until we obtain a good fit to the position of the red wing and the depth and width of the absorption profile. We assume that the emission of H β is formed independently in the accretion disk and do not model it.

TABLE 4
PARAMETERS DERIVED BY FITTING THE ABSORPTION COMPONENT OF H β

Parameters	M1-92	MWC 560
WD mass ^a (M_{\odot}).....	0.6	0.6
Rotation velocity ^a Ω_0 (rad s ⁻¹).....	3.6×10^{-6}	3.6×10^{-6}
Injection velocity V_0 (km s ⁻¹).....	590	900
Distance to the injection point Z_0 (R_{\odot}).....	0.66	0.24
Velocity dispersion V_{turb} (km s ⁻¹).....	100	50
Mass-loss rate (M_{\odot} yr ⁻¹).....	3×10^{-13}	9×10^{-12}
Magnetic field B_0 (G).....	50	3150
Density ρ_0 (g cm ⁻³).....	1.6×10^{-15}	1.7×10^{-13}

^a Adopted values.

Figure 5 shows the fit of the observed absorption component of H β in the two objects. Table 4 summarizes the obtained parameters. We have to stress that these values are obtained by trial-and-error fits and might not be unique, even though the strong relation between them assures us that the real parameters (within the assumptions of the model) are not expected to be very different than the obtained ones. Furthermore, although the parameters given in Table 4 are uncertain, we are confident that the relative values of the parameters for the two objects are valid; that is, the hydrogen column density in MWC 560 is 2 orders of magnitude higher than for M1-92.

As a final test we compare the column density obtained by the model and the value estimated from the equivalent width. In the case of MWC 560 the total hydrogen column density found in our model is $N_0 \sim 10^{22}$ cm⁻², while the column density of hydrogen in level 2 computed from Schmid et al. (2001) for H9, for example, is $N_2 > 10^{16}$ cm⁻². If we assume that $N_2/N_1 = (g_2/g_1)e^{(-10.2/kT)}$ for $T \sim 10^4$, then $N_2/N_1 \sim 10^{-6}$. Thus, the total atomic hydrogen column density is $\sim 10^{16}/10^{-6} = 10^{22}$ cm⁻², in agreement with our models. From both the equivalent widths and the fit to the profiles, the column density of the jet of M1-92 is estimated to be about 1 order of magnitude lower than that of MWC 560.

Another important difference is the estimated strength of the magnetic field. The jet of MWC 560 starts much closer to the stellar surface, which is reflected in the higher velocity of the red wing of the absorption. The magnetic field required to accelerate

this jet is also higher. If one assumes that M1-92 evolved from an object similar to MWC 560, then one can speculate that as the system evolved from higher to lower mass-loss rate, the jet became weaker and moved away from the star, with the corresponding decrease of the magnetic field.

6. NATURE OF THE BINARY SYSTEMS M1-92 AND MWC 560

6.1. Binary Nuclei

A symbiotic system consists of a white dwarf that provides H-ionizing photons and a red giant star that is transferring mass to the compact star. M1-92 is known to be a binary from its UV spectrum; the similarities between its optical spectrum and that of MWC 560 suggest the idea that it is not only a binary but also a symbiotic system.

The *IUE* archive of M1-92 contains four low-resolution spectra (LWP09614, LWP10313, SWP29786, and SWP33677), which have been reported by Feibelman & Bruhweiler (1990). For this study we have reexamined the spectra to try to determine more refined fits to the data. We combined them to obtain a single spectrum of better S/N covering the spectral range from 1100 to 3200 Å. This spectrum is shown in the left panel of Figure 6. The low resolution and low S/N, although not allowing a detailed modeling, still allow fitting a Kurucz model to it. The description is given in Kurucz (1992), and the models were obtained online.¹ We proceeded first by examining the entire collection of models and selected two regions: region A (2300–2740 Å), which is sensitive to temperature, and region B (2910–3010 Å), which is sensitive to luminosity. We compared the flux distribution of Kurucz models and adjusted the reddening to M1-92 until we reproduced the flux distribution in the two regions. The best fit was obtained with a model with $T_{\text{eff}} = 6500$ K and $\log g = 0.5$. Note that higher $\log g$ values would give too shallow an absorption in region B, while higher or lower temperatures would not reproduce the intensity of the bump at ~ 2500 Å in region A. The steps of Kurucz models are 500 K so the error in T_{eff} is of the order of 250 K. The $\log g = 0.5$ model is the one with the smallest gravity in the grid, and this value should be taken as an upper limit for the gravity of the star. The fit of the entire spectrum was obtained by

¹ See <http://kurucz.harvard.edu/grids.html>.

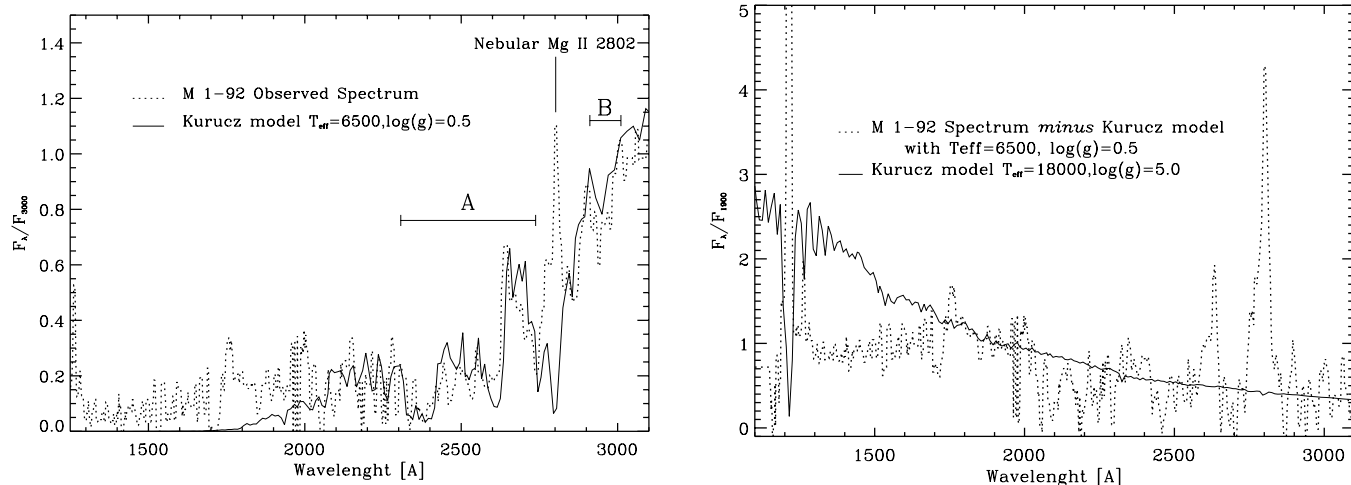


FIG. 6.—Fit to the *IUE* spectrum of M1-92. *Left*: Comparison to a $T_{\text{eff}} = 6500$ K, $\log g = 0.5$ model. Both observed and theoretical spectra are normalized to the flux at 3000 Å. The observed spectrum is dereddened with $E(B - V) = 0.1$. *Right*: Comparison of the residual intensity calculated by subtraction of a Kurucz model used in the right panel from the observed spectrum to a Kurucz model with $T_{\text{eff}} = 18,000$ K and $\log g = 5.0$ (see text).

dereddening the observed flux with $E(B - V) = 0.1 \pm 0.02$. We have to note that the slope of the UV spectrum is very sensitive to the reddening, hence the small error in this parameter. We have to stress that the model was chosen by comparison of the spectral features that are reddening independent. The reddening is calculated using the slope of the continuum. The fit of the spectral features and the reddening are independent of each other, and it is not possible to choose a different temperature for the star by just applying a different reddening.

It is seen in the left panel of Figure 6 that the emission bluer than 2000 Å is too strong for a star with $T_{\text{eff}} = 6500$ K. The right panel of Figure 6 shows the subtraction of a Kurucz model to the observed spectrum for $E(B - V) = 0.1$. The residual resembles the continuum of a blue star: our best fit is a Kurucz model with $T_{\text{eff}} = 18,000$ K and $\log g = 5.0$, as seen in the right panel of Figure 6. We should note that the fit is based mainly on the red part of the spectrum, which is dominated by the red star. The residual flux has even lower S/N than the original data, and the parameters of the fit have to be taken only as crude estimates. The blue star, if it exists, most likely has an accretion disk, and one cannot expect to fit it with a plane-parallel model as those calculated by Kurucz. Nevertheless, the low ionization of the nebula suggests a temperature of the hot star less than 20,000 K, which is in agreement with our estimate. A two-component system of similar parameters was obtained by Feibelman & Bruhweiler (1990).

6.2. Accretion Disks around the Compact Objects in Both Systems

The symbiotic star MWC 560 has shown variations in its continuum and its UV and optical line intensities. Michalitsianos et al. (1993) proposed that the quasi-periodic variations of timescales of 3–35 minutes observed in MWC 560 in some permitted low-excitation lines originate in the magnetosphere of an accretion disk.

In the case of M1-92, both the presence of the same permitted low-excitation lines as in MWC 560 and the evidence of a high-velocity jet lead us to propose that there is an accretion disk surrounding the compact object that has similar characteristics as that in MWC 560. Following this idea, we searched for variability in the three observing runs available in our data, and we found no differences at the level of confidence that the low S/N level allowed (that is, of 30% intensity in the hydrogen lines and of 20% intensity in the other features). Nevertheless, it would be important to monitor short-term changes in M1-92, for the purpose of determining whether or not there is variability in the spectrum similar to that of MWC 560.

In any case, the similarities in the spectra point to similar geometry and physical conditions for both systems, in particular for a jet being ejected by the compact star with an accreting disk. An artistic conception of the deduced structure and orientation of the systems is presented in Figure 4.

It is important to note that this hypothesized accretion disk would be a small structure surrounding the compact star of the M1-92 system and does not correspond to the much larger sized dusty torus observed by Bujarrabal et al. (1998a), which is bigger than the binary separation.

7. IS THERE AN EVOLUTIONARY SEQUENCE FROM MWC 560 TO M1-92?

While in MWC 560 the companion is an M4ep star, in the case of the PPN it is an F2 Ia star. This can indicate that the binary system in the PPN M1-92 is more evolved than that of the symbiotic star MWC 560. This agrees with the following character-

istics: (1) the faintness of forbidden emission lines in MWC 560, which can be explained if the ejected gas of the red giant has not expanded to a low enough density to emit significantly in these lines; and (2) the envelope of MWC 560 is at most $(0.5 - 1.2) \times 10^{16}$ cm, while the lobe structure of M1-92 is 4×10^{17} cm.

Eiroa & Hodapp (1989) derive a kinematical age of 1600 yr for the disk, while from the size of the molecular envelope of M1-92, a kinematical age of ~ 900 yr has been estimated by Bujarrabal et al. (1998a). On the other hand, the timescale for evolution from M to F in the giant stage for the progenitors of PNs is ~ 1200 yr (Schönberner 1983). Then one can speculate that ~ 900 years ago, the central object of M1-92 was a symbiotic system, where the red giant expelled its outer layers, formed the nebula, and at the same time evolved to a yellow giant observed today.

Our evolutionary scenario is in agreement with the model proposed by Soker & Rappaport (2000) to explain the formation of very narrow equatorial waist between the two polar lobes in bipolar PNs and bipolar symbiotic nebulae and is the most probable model for M1-92 and MWC 560. It requires the interaction of the slow wind blown by the post-AGB star with a collimated fast wind from the hot compact companion; the collimated fast wind results from accretion of the post-AGB wind into an accretion disk around the companion.

Although there are other indications of similarities between highly elongated bipolar nebulae and symbiotic Mira variables, M1-92 and MWC 560 have the further similarity that there is a jet present in both objects.

8. CONCLUSIONS

For the first time, the likeness between the spectra of M1-92, a PPN with bipolar morphology, and the symbiotic star MWC 560 has been reported, and from this similarity geometrical considerations have been inferred for the structure of M1-92.

In particular, both systems under consideration show very similar profiles in the same strong permitted lines (H I, He I, Ca II, Fe II, and Na I). These lines were explained previously for MWC 560 by a collimated fast wind along the line of sight. Although M1-92 does not have the same orientation, a similar geometry can be envisioned, if the presence of light-scattering effects from dust is taken into account. This effect gives the observer the opportunity of viewing the light from the central object through the jet, in spite of its being almost perpendicular to the observer.

From the previous discussion, the presence of a jet of material of low degree of ionization in M1-92 is strengthened. It is found that the jet has maximum velocities that range from 580 to 760 km s⁻¹ with widths of 200–450 km s⁻¹, depending on the observed line. The evidence of this jet is in agreement with the *HST* image and the prediction by Bujarrabal et al. (1998a), as well as the polarimetry measurements by Trammell et al. (1993).

It is also proposed that M1-92 corresponds to a more advanced evolutionary stage than that of MWC 560 with an estimated difference of 900–1200 yr. The connection between Mira symbiotic stars and bipolar PNs as proposed by different authors is confirmed by the similarity between MWC 560 and M1-92. The existence of a jet in both systems suggests that the white dwarf's outflow is highly collimated by a disk accreted from the mass transferred by the post-AGB companion.

The authors are grateful to Lorenzo Olguín for data reduction of MWC 560 and to Mario Livio for fruitful discussions. Support from DGAPA-IN100799, DGAPA-IN114601, and CONACyT-25451E grants is acknowledged.

REFERENCES

- Arrieta, A., & Torres-Peimbert, S. 2003, *ApJS*, 147, 97
- Bond, H. E., Pier, J., Pilachowski, C., Slovak, M., & Szkody, P. 1984, *BAAS*, 16, 516
- Bujarrabal, V., Alcolea, J., & Neri, R. 1998a, *ApJ*, 504, 915
- Bujarrabal, V., Alcolea, J., Sahai, R., Zamorano, J., & Zijlstra, A. A. 1998b, *A&A*, 331, 361
- Chentsov, E. L., Kochkova, V. G., & Mal'Kova, G. A. 1997, *Bull. Spec. Astropys. Obs.*, 43, 18
- Cohen, M., & Kuhl, L. V. 1977, *ApJ*, 213, 79
- Corradi, R. L. 1995, *MNRAS*, 276, 521
- . 2003, in *ASP Conf. Ser. 303, Symbiotic Stars Probing Stellar Evolution*, ed. R. L. M. Corradi, R. Mikolajewska, & T. J. Mahoney (San Francisco: ASP), 393
- Corradi, R. L., Mikolajewska, J., & Mahoney, T. J. 2003, *ASP Conf. Ser. 303, Symbiotic Stars Probing Stellar Evolution* (San Francisco: ASP)
- Corradi, R. L., & Schwarz, H. E. 1995, *A&A*, 293, 871
- Eiroa, C., & Hodapp, K.-W. 1989, *A&A*, 223, 271
- Feibelman, W. A., & Bruhweiler, F. C. 1990, *ApJ*, 354, 262
- Fuhr, J. R., Martin, G. A., Wiese, W. L., & Younger, S. M. 1981, *J. Phys. Chem. Ref. Data*, 10, 305
- Georgiev, L., & Koenigsberger, G. 2004, *A&A*, 423, 267
- Herbig, G. H. 1975, *ApJ*, 200, 1
- Hollis, J., & Koupelis, T. 2000, *ApJ*, 528, 418
- Iijima, T. 2002, *A&A*, 391, 617
- Kohoutek, L. 1997, *A&AS*, 125, 445
- Kolev, D., & Tomov, T. 1993, *A&AS*, 100, 1
- Kurucz, R. L. 1992, in *IAU Symp. 149, Stellar Population of Galaxies*, ed. B. Barbuy & A. Renzini (Dordrecht: Kluwer), 225
- Lee, H.-W. 2000, *ApJ*, 541, L25
- Lee, H.-W., & Hyung, S. 2000, *ApJ*, 530, L49
- Lutz, J. H., Kaler, J. B., Shaw, R. A., Schwarz, H. E., & Aspin, C. 1989, *PASP*, 101, 966
- Merrill, P. W. 1951, *ApJ*, 114, 37
- . 1961, *ApJ*, 133, 503
- Merrill, P. W., & Burwell, C. G. 1943, *ApJ*, 98, 153
- Michalitsianos, A. G., et al. 1993, *ApJ*, 409, L53
- Minkowski, R. 1946, *PASP*, 58, 305
- Morris, M. 1990, in *From Miras to Planetary Nebulae: Which Path for Stellar Evolution?*, ed. M. O. Mennesier & A. Oncent (Paris: Editions Frontières), 520
- Sanduleak, N., & Stephenson, C. B. 1973, *ApJ*, 185, 899
- Schmid, H. M., Kaufer, A., Camenzind, M., Rivinius, Th., Stahl, O., Szeifert, T., Tubbesing, S., & Wolf, B. 2001, *A&A*, 377, 206
- Schönberner, D. 1983, *ApJ*, 272, 708
- Schwarz, H. E., & Corradi, R. L. M. 1992, *A&A*, 265, L37
- Seaquist, E. R., Plume, R., & Davis, L. E. 1991, *ApJ*, 367, 200
- Soker, N., & Rappaport, S. 2000, *ApJ*, 538, 241
- Solf, J. 1994, *A&A*, 282, 567
- Tomov, T., Kolev, D., Georgiev, L., & Antov, A. 1990, *Nature*, 346, 637
- Tomov, T., Zamanov, R., Kolev, D., Georgiev, L., Antov, A., Mikolajewski, M., & Esipov, V. 1992, *MNRAS*, 258, 23
- Trammell, S. R., Dinerstein, H. L., & Goodrich, R. W. 1993, *ApJ*, 402, 249
- Trammell, S. R., & Goodrich, R. W. 1996, *ApJ*, 468, L107
- Wiese, W. L., Smith, M. W., & Glennon, B. M. 1966, *Atomic Transition Probabilities*, Vol. 1, NSRDS-NBS 4 (Washington: US Department of Commerce)
- . 1969, *Atomic Transition Probabilities*, Vol. 2, NSRDS-NBS 22 (Washington: US Department of Commerce)